Design Criteria for Si Point-Contact Concentrator Solar Cells

RONALD A. SINTON AND RICHARD M. SWANSON, MEMBER, IEEE

Abstract—**Design criteria for concentrator solar cells are presented for the highly three-dimensional case of backside point-contact solar cells. A recent new experimental result, a 28-percent efficient cell (25°C, 15-W/cm^2 incident power) is used as a case study of the dependences of the recombination components and the carrier density gradients on the geometrical design parameters. The optimum geometry is found to depend upon the intended design power density as well as the attainable physical parameters allowed by the fabrication techniques utilized. Modeling projections indicate that an ultimate efficiency of 30.6 percent (36 W/cm^2, 300 K) is achievable using the diffused emitters presently employed on these cells. Incorporation of results from the study of polycrystalline emitters could improve these efficiencies toward 31.7 percent.**

I. Introduction

SEVERAL recent studies of silicon concentrator solar cells have predicted that efficiencies up to 37 percent are possible in highly idealized cells [1]–[4]. Gray and Schwartz considered the efficiencies of a particular cell design, an interdigitated back contact cell with line diffusions, using a two-dimensional analysis [1]. Campbell and Green looked primarily at the fundamental recombination limit imposed by the Auger recombination in silicon in the highly idealized case in which other recombination components, the effects of diffusion gradients, and the resulting electric field losses present in any specific implementations were neglected [2]. The effects of an optimization of the acceptance angle for the light absorption in the cell to enhance the limits of photogeneration were also considered. Swanson developed a three-dimensional model when the point-contact design was proposed for use as a concentrator cell [3], [4]. This model was based on the experience gained in a program in which a 29-percent efficient thermophotovoltaic cell was demonstrated that utilized the point contact approach to reduce parasitic infrared absorption [5], [6]. The model predicted an idealized thermodynamic limit of 37.8 percent for silicon concentrator solar cells under an incident intensity of 36 W/cm^2 at 330 K. When the point-contact design was considered, including incomplete absorption, Auger recombination and transport losses (diffusion gradients), the upper limit to the efficiency for silicon cells was 32.3 percent at 330 K under an incident power density of 36 W/cm^2.

This paper closely follows the modeling of Swanson. Experimental results from solar cells are analyzed as case studies. The various ways in which the performance depends upon the cell geometry are displayed. Data from nonoptimal geometries are also presented in order to investigate the accuracy and limits of the model. This study utilizes measured values for all of the parameters such as surface recombination velocity, bulk lifetime, and emitter saturation currents, as well as recent evaluations of the Auger recombination in the carrier density range of interest here [7], [8].

II. The Model

The cells under consideration are fabricated on high-resistivity silicon, typically 100–400-Ω · cm n-type float zone material. Under illuminated conditions, the entire cell is highly injected except for the heavily doped emitter regions. The model considers only the lowly doped regions, and takes the emitter recombinations as a boundary condition fully characterized by the experimental emitter saturation current J_{oe}, the carrier density at the edge of the space charge region, and the area of the diffusion.

The model assumes a solution for the carrier density in the undoped region as shown in Fig. 1. In region 1, the solution is assumed to be one-dimensional; in region 2, the carrier density is assumed constant, and a three-dimensional solution is used in the collection regions, labelled region 3. The approximation of a uniform carrier density in region 2 allows the simple tractability of this modeling approach. Perpendicular to the back surface in region 2, the gradient in carrier density falls rapidly toward zero, its value at a well passivated surface. An upper limit to the effects of the neglect of these gradients could be determined by simulating a cell that is thicker by half of the depth of this region, thus taking this gradient explicitly into account. For a typical cell to be discussed in Section III, a 120-μm-thick cell operating under 36 W/cm^2 of incident power density, this causes a 0.3-percent drop in absolute efficiency (out of 28 percent). Bounds on the carrier density drop in the lateral direction, between the n$^+$ and p$^+$ contacts in region 2 can be evaluated using standard p$^+$-i-n$^+$ diode equations [10]. Since the diffusion length is much greater than the distance between contacts [8], these gradients are entirely negligible

Manuscript received November 3, 1987; revised March 9, 1987. This work was done in affiliation with the Stanford Integrated Circuits Laboratory and the Center for Integrated Systems supported by the Sandia National Laboratories under Contract 32-8112, the Electric Power Research Institute, under Contract RP-790-2, and under an Exxon Fellowship.

The authors are with the Stanford Electronics Laboratories, Stanford, CA 94305.

IEEE Log Number 8716122.

0018-9383/87/1000-2116$01.00 © 1987 IEEE

Authorized licensed use limited to: Sidley Austin LLP. Downloaded on April 28,2024 at 05:00:29 UTC from IEEE Xplore. Restrictions apply.

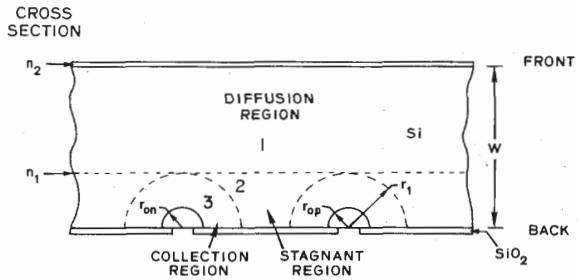

Fig. 1. A cross section of a point-contact solar cell showing the three regions considered in the modeling.

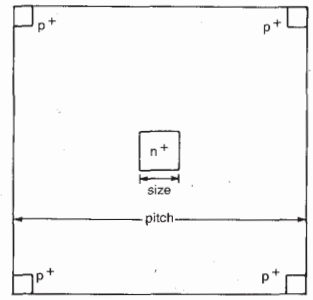

Fig. 2. A unit cell which defines the geometry of the diffusions on the backside of the wafer.

in the devices considered here at the maximum power point.

If there is no recombination or generation in the bulk, then the carrier density is described by Laplace's equation, and the boundary r_1 between the one- and three-dimensional regions can be optimized to find the best solution using variational techniques [3], [4]. The assumption of no recombination in the bulk is a very good approximation for the cell operation at the maximum power point. From the modeling of the best experimental cell to date (a 120-μm-thick cell), the quantum efficiency in the lowly doped regions of the cell is greater than 95 percent at all values of the incident power density (AM1.5) in the range of 0.1 to 36 W/cm^2. A thinner cell, 50 μm, has a base quantum efficiency greater than 97.6 percent for power densities as high as 56 W/cm^2. These figures exclude the surface and emitter recombination that are incorporated into the analysis as boundary conditions.

The modeling considers one unit cell as shown in Fig. 2, which is repeated symmetrically over the entire back surface of the solar cell. Using the notation defined by Figs. 1, 2 and Table I, a key result from the variational analysis is that the boundary between the one- and three-dimensional regions r_1 is given by

$$r_1 = \frac{P \times (D_A)}{\sqrt{8\pi}} \sqrt{\frac{1}{D_p^2} + \frac{1}{D_n^2}}. \tag{1}$$

This radius increases linearly as the spacing between contacts increases. The radius r_1 assumes a hemispherical geometry. To make the maximum use of the symmetry of the problem, the diffusions are also described as having a hemispherical radius r_{on} for the n$^+$ diffusion, which results in the same area as the actual square diffusion area (after outdiffusion) on the fabricated devices. The three-dimensional drop in carrier density from r_1 to this hemispherical space charge region edge r_{on} is given by

$$\Delta n_n = \frac{J(r_1) \times (P)^2}{4\pi q D_n} \left(\frac{1}{r_{on}} - \frac{1}{r_1}\right) \tag{2}$$

into the n-type contact and

$$\Delta n_p = \frac{J(r_1) \times (P)^2}{4\pi q D_p} \left(\frac{1}{r_{op}} - \frac{1}{r_1}\right) \tag{3}$$

for the p-type contact. P is the pitch, or spacing between identical contacts. These results are derived in [3] and [4]. Although the carrier density was previously described by an analytical approximation to the carrier density in the one-dimensional region, a numerical solution was used in this paper in order to incorporate the effects of bulk generation and recombination. This solution was constructed by implementing a stepwise integration of the diffusion equation and the continuity equation for the steady state.

$$\frac{dn}{dx} = \frac{J_n(x)}{qD_A} \tag{4}$$

and

$$\frac{dJ_n(x)}{dx} = (G(x) - R(n)). \tag{5}$$

In this one-dimensional region the total current is zero, so J_n is the flux of electrons *or* holes from the front toward the back of the cell. D_A is the ambipolar diffusion coefficient, and G and R represent the generation and recombination per unit volume. By constructing a numerical solution, the effects of the recombination are incorporated into the profile and the consequences of a carrier-density-dependent diffusion coefficient and a position-dependent photogeneration profile can then be evaluated. Although the modeling of solar cells near the maximum power point is relatively insensitive to the effects of recombination in the base on the profile, the removal of this assumption is critical for modeling the open-circuit voltage as discussed in [8].

The value for r_1, shown in (1), resulting from the analytical solution in [4] was used in this case as a reasonable approximation. In order to neglect generation and recombination in the bulk, the previous modeling assumed a worst case approximation of a delta function of generation at the sunward surface of the cell. As a numerical solution is constructed in the present work, a more general photogeneration profile can be incorporated. The generation profile chosen consists of both a delta function of generation and a uniform generation (in the one-dimensional region of the cell) with the ratio of the two chosen to give

Authorized licensed use limited to: Sidley Austin LLP. Downloaded on April 28,2024 at 05:00:29 UTC from IEEE Xplore. Restrictions apply.

TABLE I
VARIABLES

J_{ph}	Total photogenerated current
J_{term}	Terminal Current
V_{term}	Terminal Voltage
R	Recombination rate
G	Photogeneration rate
τ	Shockley-Read-Hall high-level injection lifetime
n	Carrier density, n=p in high level injection
n_{on}, n_{op}	n at the depletion edge of the n^+/p^+ diffusion.
S	Surface recombination velocity
J_{on}/J_{op}	Emitter saturation current density for the n^+/p^+ diffusion
A_n/A_p	Fraction of the total back surface area covered by n^+/p^+ diffusion
C_A	Ambipolar Auger coefficient
W	Solar cell wafer thickness
P	The pitch, or distance between diffusions of the same type, center to center.
$D_A/D_n/D_p$	Ambipolar/n-type/p-type diffusion coefficient
r_1	Boundary between 1-dimensional and 3-dimensional regions.
r_{on}/r_{op}	radius of a hemisphere of equivalent area to the experimental square diffusion.
n_1	The carrier density at r_1
$\Delta n_n/\Delta n_p$	The drop in carrier density across the 3-dimensional region near the n/p contact

the correct average point of generation as determined by an integration of the absorption of an AM1.5 spectrum as a function of depth in silicon. For a texturized cell, a determination of this average point of generation is more complex. The approach used here was to find the average point of generation for one pass of the photon spectrum through the cell thickness at the angle that would result from normal incidence onto a texturized surface of a ⟨100⟩ wafer. The rest of the photogeneration was assumed to be uniform with the total photogeneration chosen in order to obtain the total predicted by Yablonovitch and Cody [9] for texturized wafers, and modified by Campbell and Green to take into account more optimized optics [2]. The photogeneration predicted by Campbell for a 30° acceptance angle typical of many concentrator applications was used in this study as an upper limit in the evaluation of future prospects.

The carrier density is assumed to be continuous across the boundary between the region of uniform carrier density and the three-dimensional collection region, labeled regions 2 and 3. The current inside the three-dimensional region is assumed to be the photogenerated current minus the recombination current already evaluated for regions 1 and 2. An appropriate step size was chosen for the numerical integration in the one-dimensional region such that no sensitivity in the efficiency was seen to three significant figures.

Once the carrier density has been modeled, the terminal current and voltage can be evaluated. The terminal current will be given by the total photogeneration current J_{ph} minus the total recombination current, which depends upon the carrier density throughout the solar cell [4].

$$J_{\text{term}} = J_{ph} - \left[\frac{q}{\tau} \int n(x)\, dx + \frac{qS \int n dA}{\int dA} + J_{op} A_p \left(\frac{n_{op}}{n_i}\right)^2 + J_{on} A_n \left(\frac{n_{on}}{n_i}\right)^2 + qC_a \int n^3(x)\, dx \right]. \quad (6)$$

This equation contains the assumptions made for each of the recombination mechanisms. The bulk Shockley–Read–Hall recombination in the first term is assumed to be linearly dependent upon the carrier density. The surface recombination is also assumed to be linear in the carrier density and must be integrated over the carrier densities at both the front and back lightly doped n-type surfaces. The third and fourth terms result from the emitter recombination. This recombination depends on the emitter saturation current J_{on} for the n^+ diffusion, the fraction of the backside area covered by these diffusions A_n, and the square of the carrier density at the edge of the space-charge region in the lowly doped base. The last term is the bulk ambipolar Auger recombination, which is assumed to depend upon the carrier density cubed [8].

The voltage can be calculated from the carrier densities at the two space-charge region edges with additional terms due to the voltage drops from the three-dimensional gradients into the contacts. The resulting terminal voltage is [3], [4]

$$V_{\text{term}} = \frac{2kT}{q} \ln \left(\frac{n_{on} n_{op}}{n_1 n_i}\right). \quad (7)$$

An interesting way to look at this equation for terminal voltage is as

$$V_{\text{term}} = \frac{2kT}{q} \ln \left[\left(\frac{n_1}{n_i}\right)\left(1 - \frac{\Delta n_n}{n_1}\right)\left(1 - \frac{\Delta n_p}{n_1}\right)\right]. \quad (8)$$

In this way, the effect of the three-dimensional drops in carrier density on the terminal voltage is clearly displayed by the two correction terms in the argument of the natural logarithm. This conclusion follows since this equation without these two correction terms would result if the ef-

Authorized licensed use limited to: Sidley Austin LLP. Downloaded on April 28,2024 at 05:00:29 UTC from IEEE Xplore. Restrictions apply.

fects on the voltage of the carrier density gradients in the cell were neglected. Equation (8) contains both the loss in voltage due to the decreased carrier concentrations from the gradient and the voltage drop, which was evaluated by integrating the electric fields through this region [4]. Note that the conductivity modulation will increase the absolute carrier density n_1 thus reducing the voltage drops.

Some of the effects of the numerical integration and assumptions about the photogeneration profile can be summarized by their effect upon the efficiency of a test case, a 120-μm-thick solar cell as discussed in Section III. Under an incident power density of 36 W/cm^2, the modeling from [4] predicts an efficiency of 27.66 percent. By incorporating the numerical integration into the one-dimensional region but maintaining a delta function of photogeneration at the front surface, the efficiency improves to 27.75. Including an approximate photogeneration profile taking the texturization into account, this efficiency is increased to 27.94 percent. The effect on the carrier density profile is small at the maximum power operating point. Compared to the texturized case, the previous modeling would predict carrier densities higher at the front of the cell (8 percent in the above case) and lower at the back surface of the cell (by 6 percent at the p^+ depletion region edge).

III. Modeling of a Baseline Cell

By applying this model to analyze data from fabricated solar cells, a baseline case can be established from which future designs can be extrapolated. Data of efficiency versus incident power density is shown for a recent cell run in Fig. 3. This 120-μm-thick solar cell is very similar to those reported in [11] except that a 4-μm aluminum metallization was used to reduce the series resistance to half that of the previous 2-μm-thick grid. These results were measured at a cell temperature of 25°C. The cell is 28-percent efficient in a range from 4 to 15 W/cm^2 (40 to 150 suns). At the highest incident power measured, 53 W/cm^2, it is still 25.4-percent efficient. At the design concentration of 36 W/cm^2, it is 26.5-percent efficient. The test procedure is detailed in [20].

This result can be modeled with the parameters shown in Table II. The parameters shown have been determined using photoconductivity decay methods [12] and open-circuit voltage steady-state and decay measurements [8]. The total photogeneration in these simulations was assumed to be the experimental 0.42 A per incident watt, which was measured as short-circuit current under low incident power densities. Fig. 4 shows the contribution of each recombination mechanism at the maximum power point as a function of the incident power density. For a wide range of power densities, between 0.5 and 20.0 W/cm^2, the recombination at the maximum power point is dominated by the emitter recombination. This is despite the fact that the emitter area has been reduced by a factor of 10 from what it would be in a conventional p-i-n concentrator solar cell. The diffusion mask windows were 10 × 10 μm on a 50-μm pitch as shown in Fig. 2. After outdiffusion of the dopants, the diffusion area at the surface is estimated to be 16 × 16 μm [13]. Above 20 W/cm^2, the recombination is dominated by the bulk Auger recombination.

The key physical quantity that determines the contribution of each recombination mechanism is the carrier density as a function of position in the cell. The modeled carrier density profile is shown in Fig. 5 under open circuit, maximum power point, and short-circuit current

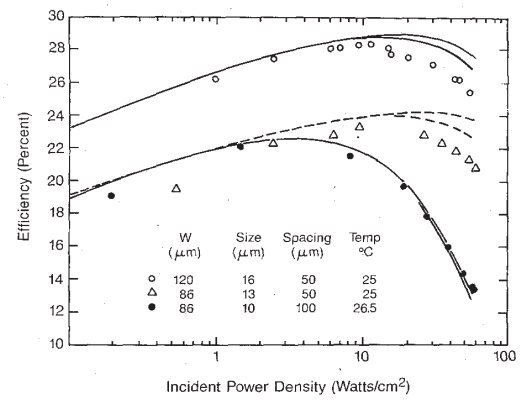

Fig. 3. The efficiencies versus the incident intensity for three geometries of a solar cell. The cell thickness, the diffusion size, and spacing (pitch) is given. Only the top cell is texturized. The curves are from the model. The lower branch of each curve includes a correction for the calculated lumped series resistance for the metallization on each cell.

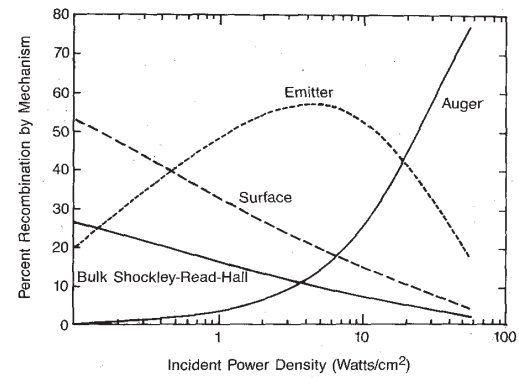

Fig. 4. The modeled recombination components as a function of the power density incident upon a 120-μm-thick cell for the maximum power point at each incident power.

TABLE II
Modeling Parameters

τ	3 milliseconds
S	7.5 cm/sec
J_{on}, J_{op}	4.5×10^{-13} Amps/cm^2
C_A	1.66×10^{-30} cm^6/sec[8]
D_A	$D_A = 18$ cm^2/sec[21,22]
D_n/D_p	Majority carrier mobility data. [23]/[24].
n_i	$3.563 \times 10^{16}(T^{1.5})exp(-6980/T)$*

*The activation energy of this expression was taken from H. D. Barber, "Effective mass and intrinsic concentration in silicon," *Solid-State Electron.*, vol. 10, pp. 1039–1051, 1967. The prefactor is a fit which gives the value at 300°C, 1.45×10^{10}/cm^3, commonly used in modeling.

Authorized licensed use limited to: Sidley Austin LLP. Downloaded on April 28,2024 at 05:00:29 UTC from IEEE Xplore. Restrictions apply.

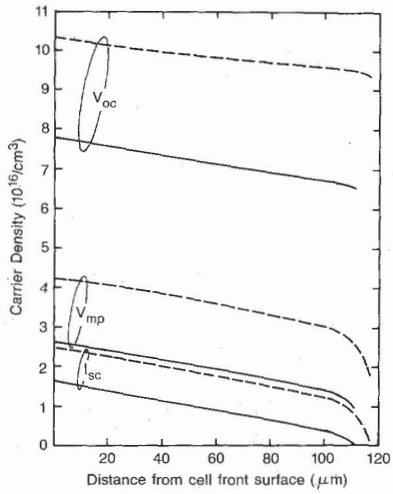

Fig. 5. The modeled carrier density profile n as a function of position from front to back in the solar cell along a line into a p^+ contact. Curves are shown for cells with 8-μm^2 diffusions (dashed curve) and 20 μm diffusions (solid curve), both on a 50-μm pitch. 10 W/cm^2, 300 K.

conditions for cells with the emitter spacing and cell thickness discussed above and at an operating incident power density of 10 W/cm^2. For a fixed pitch of 50 μm, these operating conditions are displayed for square diffusion sizes of 8 and 20 μm. The carrier density is highest at the front of the cell where most of the photogeneration occurs. The carriers then diffuse down a gradient in carrier density to the back of the cell where they are collected at the contacts. The profiles shown here are from a cross section that passes into a p^+ diffusion.

By reducing the emitter recombination by decreasing the emitter area, higher average carrier densities result. The steep gradients near the contacts when current is drawn from the cell result from the increased current density. At the contact, the current density will approach the total photogenerated current divided by the back surface coverage fraction for each emitter type. From (2) and (3), the drop in carrier density is inversely proportional to the diffusion size. It is greater for the smaller coverage fraction and partially negates the gains in carrier density due to the decreased emitter recombination. These steep gradients also result in non-negligible electric fields that decrease the terminal voltage. This effect on the voltage is seen in (8) where the ratio of the three-dimensional carrier density drop to the absolute carrier density enters into the expression for the terminal voltage. Because the average carrier density in the cell increases as the emitter coverage fraction decreases, the recombination due to surface, bulk Shockley–Read–Hall, and Auger recombination increases. In summary, a decreased emitter recombination obtained by reducing the emitter coverage fraction is opposed by the increased recombination from the other mechanisms due to the three-dimensional carrier density drop as well as by electric fields that result from small emitter coverage fractions.

Another way to look at this same effect is to plot the voltage and current at the maximum power points as a function of this emitter size at a fixed emitter spacing. This modeling result is shown in Fig. 6. Using a large emitter coverage fraction as a reference, 24 × 24 μm square emitters on a 50-μm pitch, the normalized maximum power point voltage, current, and efficiency are plotted for varying diffusion sizes at an illumination intensity of 10 W/cm^2. The current, a measure of the quantum efficiency, is reduced monotonically as the diffusion size is reduced. The voltage is increased at first as the emitter recombination is reduced but eventually begins to decrease as the combined effects of the carrier loss due to other recombination mechanisms and the voltage drop due to the very high current densities near the contacts set in. The normalized efficiency indicates that an optimum coverage fraction exists at this spacing and incident power. This optimum is for diffusions between 10 and 15 μm on a side.

The same effect of reduced quantum efficiencies and increased voltage drops can account for the efficiencies versus incident intensities shown for several different geometries in Fig. 3. Each modeling curve has two branches, the lower of the two contains a correction for the lumped series resistance calculated for the metallization used on each particular cell. The data points near the top curve are from the best cell to date as discussed above with 16 by 16 μm diffusions on a 50-μm pitch. The two lower sets of data are for a cell with 13 by 13 μm diffusions on a 50-μm pitch (center) and 10 by 10 μm on a 100-μm pitch (lower data). The cells did not have texturized front surfaces and therefore have much lower efficiencies due to the decreased photogeneration. Both cells were 86 μm thick, differ only in this emitter coverage fraction, and were processed side by side with consistent results on cells from two wafers of each geometry. By measuring the short-circuit current per incident watt at low incident power as the photogeneration (assuming unity quantum efficiency), the efficiencies can be modeled with the parameters from Table II. The short-circuit currents are 0.42 A per incident watt for the texturized cell and 0.35 A per incident watt for the other two cells. The cell with the smallest coverage fraction falls off in efficiency most rapidly at the highest incident intensities. This is due to the very large carrier density drops into the contacts that result in low terminal voltages and very high average carrier densities. As discussed above, these high densities increase the Auger recombination so that the quantum efficiencies of these cells are very poor compared to the cells with the larger coverage fractions. In contrast to the current, the open-circuit voltages are always better in the cell with the smaller coverage fraction because the three-dimensional gradients play a very small role when no current being drawn from the terminals [8].

Notice that, in the modeling for Fig. 3, no free parameters were adjusted to obtain a good "fit" at the maximum power point. Rather, the recombination parameters were those from Table II, obtained through independent

Authorized licensed use limited to: Sidley Austin LLP. Downloaded on April 28,2024 at 05:00:29 UTC from IEEE Xplore. Restrictions apply.

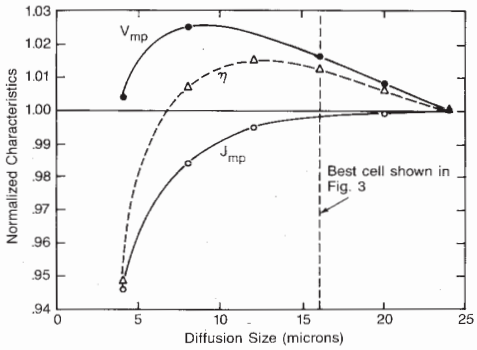

Fig. 6. The modeled normalized maximum power point voltage, current, and efficiency as a function of the square diffusion size for a 50-μm pitch. This is for a 120-μm-thick cell at 10 W/cm^2, 300 K.

measurements. The discrepancies at very high incident power densities could be due in part to an inadequate description of the metallization series resistance or a non-negligible contact resistance. Typical values for the specific contact resistivities are 1–3 $\Omega \cdot$ cm^2 for the n- and p-type contacts, each of which has an area of 5 by 5 μm.

IV. Future Advances

Several improvements can be projected that will result in higher efficiencies than those demonstrated at this time. Fig. 4 indicates that, at incident power densities above 20 W/cm^2, the Auger and emitter recombination are the dominant parasitic losses. The emitter recombination cannot be reduced much further due to the detrimental effects of the high gradients near the terminals that result from this approach. However, the effect of the Auger recombination can be reduced. The loss of quantum efficiency in thick cells due to this recombination is well documented [13]. Since the Auger coefficient is a volume-dependent recombination, efficiencies will improve as the cell becomes thinner up until a point where photogeneration is lost due to the weak absorption of silicon for light that is near the bandgap in energy. This trade-off has previously been considered for the case that neglected the diffusion gradients and non-Auger recombination [2]. For an acceptance angle of 30°, typical for Fresnel concentrator systems, the maximum photogeneration is 0.432 A per watt of incident power for an AM1.5 spectrum in a 50-μm-thick wafer, which was found to be the optimum thickness. Recent experiments [7], [8] indicate that the Auger coefficient for carrier densities less than 2×10^{17} cm^{-3} is four times higher than what had been assumed in [2]. This revised coefficient would drive this optimum thickness toward even thinner cells, but these would be difficult to fabricate with the existing process.

For the case of this cell thickness and responsivity, an optimum point contact geometry can be found. Figs. 7 and 8 are contour plots of the efficiency resulting from different diffusion spacings and sizes for the baseline process and physical parameters from Table II. At 10 W/cm^2 (300 K), the projected efficiency is about 30.0 percent as shown in Fig. 7. Although higher efficiencies than this

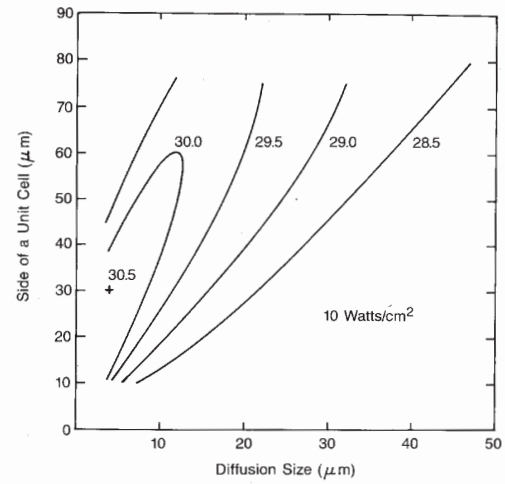

Fig. 7. Modeled contours of constant efficiency as a function of diffusion spacing (pitch) and square size. The cell is 50 μm thick and the incident intensity is 10 W/cm^2, 300 K.

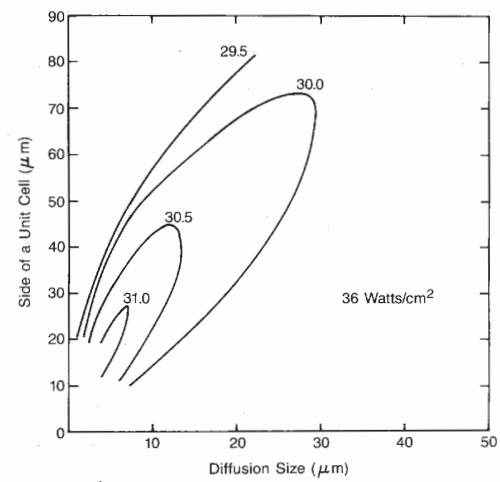

Fig. 8. Contours of constant efficiency at 36 W/cm^2.

could be attained for very small diffusion sizes, the emitters currently fabricated require deep diffusions in order to obtain the lowest possible emitter saturation currents given the infinite surface recombination at the silicon–aluminum interface. These diffusions are about 4 μm deep in the current process [8], [13], limiting accessible dimensions to more than 10 μm including the outdiffusion. The contours show a fairly sharp optimum with respect to diffusion size for a given spacing, with the optimum diffusion size giving a cell efficiency about 2 percent better (absolute) than the limit as the diffusions approach full coverage of the backside.

At 36 W/cm^2, attainable efficiencies are between 30.5 and 31 percent. The optimum with respect to the diffusion size becomes much less sharp at high incident intensities because the three-dimensional effects that oppose the use of small coverage fractions become more extreme at high

Authorized licensed use limited to: Sidley Austin LLP. Downloaded on April 28,2024 at 05:00:29 UTC from IEEE Xplore. Restrictions apply.

current densities. Note that these efficiencies were found assuming a predicted photogeneration, that has not yet been demonstrated (0.432 A/(incident watt) in a 50-μm cell. However, these results can be scaled once the experimental photogeneration for any proposed configuration is determined. The highest experimental value is that reported for the 120-μm cell shown in Fig. 3, at 0.42 A per incident watt.

The most important design rule is to choose the correct coverage fraction for each emitter type while utilizing the smallest possible dimensions. This criteria can be applied to other possible geometries. Consider line diffusions as in the interdigitated back contact solar cell [14]–[16], but with a spacing of undoped oxide–silicon interface between the n^+ and p^+ lines in order to attain an optimum emitter coverage fraction. At a fixed emitter coverage fraction and minimum emitter dimension, the carrier density drop analogous to that given by (2) and (3) is much larger in the two-dimensional case. In addition, to achieve small (10-percent) emitter coverage fractions, the diffusion lines must be spaced distances comparable to or greater than the wafer thickness. Hence, the point-contact geometry is a prefered method to reduce the emitter area given the limitations of the present technology. However, in an experimental comparison of optimized line and point contact cells, no difference in efficiency was observed within the experimental measurement error, although the experiment was not considered conclusive on this point [17].

It is interesting to project what should be possible if the best available emitter technology were applied to point-contact cells rather than the diffused emitters from the current process. Results from semi-insulating polysilicon emitters indicate that emitter saturation currents of 1.2×10^{-14} W/cm^2 are possible for n-type emitters and 3.5×10^{-13} for p-type at 300 K [18]. If these results are applied to the 50-μm-thick solar cell, efficiencies of 31.5 percent are predicted. This is for a 40-μm pitch with 24-μm n-type contacts and 12-μm p-type contacts. A plot of efficiency versus incident intensity is shown for this cell in Fig. 9. Also shown is the projected performance of an optimized cell that uses the diffused emitters already demonstrated. This cell has 12-μm square contacts for both the n- and p-type emitters and has an efficiency of 30.6 percent at the design point of 36 W/cm^2, 300 K.

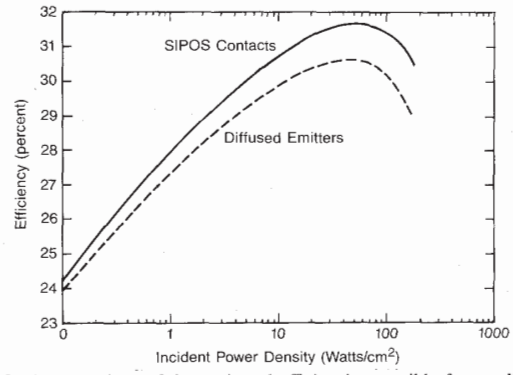

Fig. 9. A comparison of the projected efficiencies possible for a cell incorporating SIPOS emitters (solid curve), compared to projections for diffused emitters as used to date (dashed curve).

V. Conclusions

Point-contact silicon solar cells have attained a maximum efficiency of 28 percent at 25°C and 15 W/cm^2 of incident power. With a universal set of parameters fixed by independent measurements, a simplified three-dimensional model is demonstrated to be in agreement with data from a variety of cell geometries to within 1 percent in absolute efficiency for a range of incident power densities from 0.5 to 60 W/cm^2. An application of this model to a study of the recombination in the cell indicates that emitter recombination will be the major limiting factor in this cell design. This will only become evident on thinner cells than those demonstrated to date. The reduction of this recombination by shrinking the emitter coverage fraction results in high local current densities. A compromise between these two effects determines an optimum design. The efficiency can be improved by 2 percent (absolute) to 30.6 percent by reducing the cell thickness and further optimizing the cell optics. When a cell incorporating the lowest recombination emitters available is modeled, the result is an efficiency improvement to above 31.5 percent.

Acknowledgment

The authors wish to thank S. Beckwith for skillful cell fabrication. The clarity and precision of this manuscript was improved through the comments of the reviewers and E. Crabbé.

References

[1] J. L. Gray and R. J. Schwartz, "Why don't we have a 30% efficient silicon solar cell?," in *Proc. 18th IEEE Photovoltaic Specialist Conf.*, pp. 568–572, Oct. 1985.
[2] P. Campbell and M. A. Green, "The limiting efficiency of silicon solar cells under concentrated sunlight," *IEEE Trans. Electron Devices*, vol. ED-33, no. 2, pp. 234–239, Feb. 1986.
[3] R. M. Swanson, "Point-contact silicon solar cells," Electric Power Research Institute Rep. AP-2859, May 1983.
[4] ——, "Point-contact solar cells; modeling and experiment," *Solar Cells*, vol. 7, no. 1, pp. 85–118, Mar. 1986.
[5] ——, "Recent developments in thermophotovoltaic conversion," in *IEDM Tech. Dig.*, p. 186, Dec. 1980.
[6] ——, "Silicon photovoltaic cells in TPV conversion," Electric Power Research Institute Interim Rep., Palo Alto, CA, Dec. 1979.
[7] E. Yablonovitch and T. Gmitter, "Auger recombination at low carrier densities," *Appl. Phys. Lett.*, vol. 49, no. 10, p. 587, Sept. 1986.
[8] R. A. Sinton and R. M. Swanson, "Recombination in highly-injected silicon," *IEEE Trans. Electron Devices*, vol. ED-34, no. 7, pp. 1380–1389, July 1987.
[9] E. Yablonovitch and G. D. Cody, "Intensity enhancement in texturized optical sheets for solar cells," *IEEE Trans. Electron Devices*, vol. ED-29, no. 2, p. 300, Feb. 1982.
[10] S. K. Ghandi, *Semiconductor Power Devices*. New York: Wiley, 1977, pp. 110–116.

Authorized licensed use limited to: Sidley Austin LLP. Downloaded on April 28,2024 at 05:00:29 UTC from IEEE Xplore. Restrictions apply.

[11] R. A. Sinton, Y. Kwark, J. Y. Gan, and R. M. Swanson, "27.5% silicon concentrator solar cells," *IEEE Electron Device Lett.*, vol. EDL-7, no. 10, Oct. 1986.
[12] D. E. Kane and R. M. Swanson, "Measurement of the emitter saturation current by a contactless photoconductivity decay method," in *Proc. IEEE 18th Photovoltaic Specialist Conf.*, p. 578, Oct. 1985.
[13] R. Sinton, Y. Kwark, P. Gruenbaum, and R. M. Swanson, "Silicon point contact concentrator solar cells," in *Proc. 18th IEEE Photovoltaic Specialist Conf.*, pp. 61–65, Oct. 1985.
[14] M. D. Lammert and R. J. Schwartz, "The interdigitated back contact solar cell: A silicon solar cell for use in concentrated sunlight," *IEEE Trans. Electron Devices*, vol. ED-24, no. 4, Apr. 1977.
[15] C. M. Garner, R. D. Nashby, and F. W. Sexton, "An interdigitated back contact solar cell with high-current collection," *IEEE Electron Device Lett.*, vol. EDL-1, no. 12, Dec. 1980.
[16] P. Verlinden, F. Van der Wiele, G. Steheling and J. P. David, "An interdigitated back contact solar cell with high efficiency under concentrated sunlight," in *Proc. 7th European Photovoltaic Solar Energy Conf.* (Sevilla, Spain, Oct. 1986), to be published.
[17] R. A. Sinton, "Device physics and characterization of silicon point-contact solar cells," Ph.D. dissertation Stanford Univ., Stanford CA, pp. 38–44, Mar. 1987.
[18] Y. Kwark, R. A. Sinton, and R. M. Swanson, "Low J_0 contact structures using SIPOS and polysilicon films," in *Proc. 18th IEEE Photovoltaic Specialist Conf.* (Las Vegas, NV), pp. 787–791, Oct. 1985.
[19] R. A. Sinton, Y. Kwark, S. Swirhun, and R. M. Swanson, "Silicon point contact concentrator solar cells," *IEEE Electron Device Lett.*, vol. EDL-6, no. 8, pp. 405–407, Aug. 1985.
[20] R. A. Crane, R. A. Sinton, R. R. King, and R. M. Swanson, "A high concentration solar cell test facility," in *Proc. IEEE 18th Photovoltaic Specialist Conf.* (Las Vegas, NV), pp. 963–966, Oct. 1985.
[21] I. V. Grekhov and L. A. Delimova, "Ambipolar diffusion coefficient in the case of electron-hole scattering in silicon," *Sov. Phys. Semicond.*, vol. 14, no. 8, Aug. 1980.
[22] D. E. Kane and R. M. Swanson, to be published.
[23] W. R. Thurber, R. L. Mattis, Y. M. Liu, and J. J. Filliben, "Resistivity-dopant density relationship for phosphorus-doped silicon," *J. Electrochem. Soc.*, vol. 127, no. 8, p. 1807, Aug. 1980.
[24] W. R. Thurber, R. L. Mattis, Y. M. Liu, and J. J. Filliben, "Resistivity-dopant density relationship for boron-doped silicon," *J. Electrochem. Soc.*, vol. 127, no. 10, p. 2291, Oct. 1980.

Ronald A. Sinton was born in Denver, CO, in February 1959. He received the B.S. degree in engineering physics from the University of Colorado, Boulder, in 1981. He recently completed the Ph.D. degree in applied physics at Stanford University.

He is now a Research Associate at Stanford University. His research involves the development and device physics characterization of concentrator solar cells that operate under high-level injection conditions.

*

Richard M. Swanson (S'67–M'78) was born in Davenport, IA, on May 13, 1945. He received the B.S.E.E. and M.S.E.E. degrees from Ohio State University in 1969 and the Ph.D. degree from Stanford University in 1974. His dissertation research concerned the modeling and fabrication of complementary MOS integrated circuits for micropower applications and resulted in the theories and first experimental data on threshold adjustment by ion implantation and the operation of MOS transistors in the "weak inversion" regime. He was a National Science Foundation fellow while at Stanford.

While finishing his dissertation, he worked at Hewlett-Packard Laboratories, developing silicon-on-insulating-substrate technology. He received an IBM post-doctoral fellowship in 1974 at Stanford University to study techniques for solar-electric power generation. In 1976, he joined the faculty at Stanford as an Assistant Professor of Electrical Engineering and obtained funding from the Electric Power Research Institute to research thermophotovoltaic energy conversion for solar applications. Since then he has been actively involved in photovoltaics research. He is presently an Associate Professor of Electrical Engineering at Stanford University and heads a photovoltaics research team consisting of nine doctoral students, a research associate, an R&D engineer, and a processing technician. He has published over 50 technical papers.

Dr. Swanson is a member of the American Physical Society, the Electrochemical Society, the Electrochemical Society, the AAAS, the International Solar Energy Society, Sigma Chi, Tau Beta Pi, and Eta Kappa Nu.

Authorized licensed use limited to: Sidley Austin LLP. Downloaded on April 28,2024 at 05:00:29 UTC from IEEE Xplore. Restrictions apply.